Journal of Building Engineering 104 (2025) 112405

Contents lists available at ScienceDirect

Journal of Building Engineering

journal homepage: www.elsevier.com/locate/jobe

A hybrid data-driven Co-simulation approach for enhanced integrations of renewables and thermal storage in building district energy systems

Youssef Elomari [a,b,*], Giorgos Aspetakis [a], Carles Mateu [b,c], Adedamola Shobo [b], Dieter Boer [b], M. Marín-Genescà [b], Qian Wang [a,d]

[a] Department of Civil and Architectural Engineering, KTH Royal Institute of Technology, Stockholm, 10044, Sweden
[b] Departament d'Enginyeria Mecànica, Universitat Rovira i Virgili, Av. Paisos Catalans 26, 43007, Tarragona, Spain
[c] Department of Computer Science and Industrial Engineering, University of Lleida, 25001, Lleida, Spain
[d] Uponor AB, Hackstavägen 1, Västerås, 721 32, Sweden

ARTICLE INFO

Keywords:
Co-simulation framework
Multi-objective optimization
District energy system
Deep reinforcement learning
Rule-based control

ABSTRACT

Increasing the share of renewables is crucial for accelerating the sustainable transitions of modern building and district heating systems. This study develops a hybrid co-simulation framework, integrating a Python-based model with an established district energy system (DES) TRNSYS model, to optimize the design and control of on-site renewables such as photovoltaic panels (PV), solar thermal collectors, a water-to-water heat pump, seasonal thermal storage, a domestic hot water tank, and auxiliary heaters. The methodology combines diverse simulation tools and data-driven control sequences, enabling interaction across system components for enhanced energy efficiency and performance. The findings indicate that the optimized framework reduces net present cost by approximately 14 % and environmental impacts by 11 %. The data-driven controls further minimized temperature deviations significantly better than traditional Rule-Based Controls, achieving nearly optimal comfort levels with minimal environmental impact. The developed co-simulation enhances energy efficiency and intelligent controls in building applications, minimizes environmental impacts, and effectively covers the energy demand in building and districts (building clusters). These findings highlight the essential role of advanced hybrid co-simulation frameworks in improving DH system design and control, emphasizing their potential for sustainable urban energy transitions.

Nomenclature

A_{COL}	total aperture area of solar collectors (m^2)
A_{PV}	total aperture area of photovoltaic collectors (m^2)
β_{COL}	inclination angle of the solar collectors (^{o})
IIC	initial investment cost (€)
OC	total discounted operational cost (€)
RC	total discounted replacement cost (€)
DVE_k	design variable of equipment unit k

(*continued on next page*)

* Corresponding author. Department of Civil and Architectural Engineering, KTH Royal Institute of Technology, Stockholm, 10044, Sweden.
E-mail address: yelo@kth.se (Y. Elomari).

https://doi.org/10.1016/j.jobe.2025.112405
Received 18 December 2024; Received in revised form 12 March 2025; Accepted 18 March 2025
Available online 19 March 2025

(*continued*)

$CEPCI^{year\ A}$	chemical engineering plant cost index in the base year
$CEPCI^{year\ B}$	chemical Engineering Plant Cost Index in the installation year
Con_{SST}	purchase cost of the construction material of the seasonal storage tank (€)
C_M	annual cost of equipment unit k (€)
C_P	annual operational cost of a pump (€)
c_p	specific heat capacity (kJ/kg. k)
c_e	electricity price (€)
c_f	natural gas price (€)
d	annual discount rate (%)
DAM_d	indicator result for damage category d
BMF_k	bare module factor of equipment unit k
FC_{AUX}	contribution of the auxiliary heater as a percentage of the maximum heating load (%)
$f_c(x)$	original objective function [NPC(x) or RCP(x)]
h_{conv}	convective heat transfer coefficient to the air W/(m^2·K)
HDR_{SST}	seasonal storage tank aspect ratio (m/m)
HDR_{DHWT}	domestic hot water storage aspect ratio (m/m)
i	annual inflation rate (%)
i_f	annual inflation rate of natural gas (%)
i_e	annual inflation rate of electricity (%)
$\dot{m}$	mass flowrate of the recirculating water pumps (kg/s)
NPC	net present cost (€/MWh)
PCE_k	purchase cost of equipment unit k (€)
PWF_n	present worth factor of periodic future cash flows (−)
PVF_n	present value factor of single future cash flow at the beginning of nth time period (−)
$\dot{Q}_{SOL}$	useful energy rate received by the solar collector field (MW)
$\dot{Q}_{SST\ loss}$	heat loss rate through the seasonal storage tank (MW)
$\dot{Q}_{DHW\ loss}$	heat loss rate through the domestic hot water storage tank (MW)
$\dot{Q}_{HE}$	heat transfer rate through the heat exchanger (MW)
$\dot{Q}_{AUX}$	duty of auxiliary heater (MW)
$Q_{SH\ load}$	total space heating demand (MWh)
$Q_{DHW\ load}$	total domestic hot water demand (MWh)
$Q_{SST\ loss}$	total energy losses through the seasonal storage tank (MWh)
RCP	ReCiPe 2016 aggregated impact factor (Pt/MWh)
SF_{DHW}	annual solar fraction for the DHW distribution circuit (%)
SF_{SH}	annual solar fraction for the SH distribution circuit (%)
V_{DHWT}	volume of the domestic hot water tank (m^3/MWh/a)
V_{SST}	volume of the seasonal storage tank (m^3/MWh/a)
$y_{predict.i}$	predicted value
$y_{data.i}$	actual value
***Greek* symbols**	
α_{CF}	factor of contingency charges and fees
α_k	purchase cost coefficient of equipment unit k
β_k	purchase cost exponent of equipment unit k
η_{COL}	solar collector field efficiency (%)
η_{DHWT}	domestic hot water storage tank efficiency (%)
δ_d	normalization factor for damage category d
ε_d	weighting factor for damage category d
Abbreviations	
ANN	artificial neural network
AUX	auxiliary heater fueled by natural gas
COL	solar collector field
DHW	domestic hot water
DHWT	domestic hot water storage
DL	deep learning
DRL	deep reinforcement learning
HE	heat exchanger
HEM	home energy management
HVAC	heating, ventilation, and air conditioning
LCA	life cycle assessment
LCC	life cycle cost
LQR	linear-quadratic regulator
MOO	multi-objective optimization
MPC	model predictive control
DES	district energy system
SH	space heating
SST	seasonal storage tank
RBC	rule-based control
RL	reinforcement learning
TES	thermal energy storage
TRNSYS	transient system simulation program

(*continued on next page*)

(*continued*)

Indices	
d	damage category
i	elementary factor
k	equipment unit

1. Introduction

In the European Union, the energy consumption of buildings accounts for up to 40 % of the total energy usage [1], enhancing building energy efficiency a crucial element of the EU's decarbonization agenda [2]. District energy systems (DES) are comprised of a collection of buildings sharing a facility that supplies the thermal energy demand (heating and cooling) and electricity. District Heating (DH) currently supplies approximately 13 % of the EU's thermal energy needs [3] and has undergone significant evolution to lower operational temperatures [4]. This evolution has been marked by the adoption of 4th and 5th generation district heating technologies (4GDH, 5GDH), which operate efficiently at temperatures ranging from 45 °C to 55 °C and below [5,6]. This ongoing shift continues to facilitate the extensive integration of low-grade energy sources, such as distributed renewable energy systems (RES), waste heat from industrial plants and data centers into urban heating networks. The 4th and 5th generation DH systems are increasingly acknowledged as crucial technologies for the effective and cost-efficient decarbonization of Europe's energy landscape [5–7].

In the complex landscape of DH and multi-energy systems simulations, the need for multi-domain approaches is critical to effectively address challenges of complicated systems [8,9]. The challenge in traditional single-discipline simulation environments lies in their limitations with modeling comprehensive systems that include various energy sources, heating and electrical network, and buildings' HVAC system [8].

To overcome these hurdles, co-simulation facilitates the integration of multiple simulation tools and domains, thus providing a detailed and accurate representation of the entire DES system along with all associated subsystems [10]. Co-simulation's advantage lies in its flexibility and modularity, which allow for the integration of domain-specific models and simulation tools that can be tailored to the unique characteristics of each subsystem [11]. This adaptability is crucial for modeling the interdependencies and feedback loops among the different components of the sub-system, thereby offering insights into behaviors and interactions that may be overlooked with single-domain simulations [12]. Its flexibility, scalability, and distributed nature make it a well-suited approach for simulating future energy systems [13]. The introduction of co-simulation frameworks into DH systems enhances the accuracy of simulations and optimizes control strategies. By facilitating real-time data exchange and dynamic interaction between various system components, co-simulation enables the effective implementation of advanced control techniques.

As for traditional control methods, Rule-based control (RBC) has long been employed in HP systems for DH due to its straightforward implementation and operational simplicity [14]. RBC functions on a set of predefined rules aimed at achieving basic operational goals like maintaining temperature setpoints and flow rates [15]. While these methods are effective in steady-state, they fall short in addressing dynamic and fluctuating demands typical of 4-5GDH. For instance, Thygesen and Karlsson [16] proposed a RBC strategy for PV-HP systems for domestic hot water storage, achieving a 7 % increase in the annual self-consumption rate. Allison et al. [17] presented an RBC for an exhaust HP with shifting operation modes, achieving relatively low energy performance but satisfactory thermal comfort. M.H. Abokersh et al. [18] conducted a RBC of an integrated HP; the results showed that the heating system's total electrical consumption varied by 10 % between the best and worst scenarios, and a life cycle cost of up to 67.12 Euro/MWh. Katsavounis et al. [19] demonstrated that while RBC can maintain comfort levels in residential HP systems, its inability to adapt to real-time changes leads to suboptimal energy use and higher operational costs. Newer control methods, such as Model predictive control (MPC) outperform RBC by not only minimizing peak electricity demand but also ensuring better thermal comfort [14,20], thereby underscoring the limitations of RBC in optimizing HP performance in dynamic environments.

MPC is widely regarded as a more advanced and effective control strategy for HP systems, leveraging predictive models to optimize system performance over a defined horizon. Studies such as Lie-Jensen et al. [21] and Verrilli et al. [22] illustrate MPC's ability to integrate thermal energy storage, manage fluctuating loads, and achieve substantial cost savings [23]. However, MPC is not without its limitations. Its implementation requires accurate energy system models and substantial computational resources, which can pose practical challenges, especially in large-scale or complex systems [14,24,25]. Moreover, MPC frameworks often demand real-time data processing and frequent system parameter updates, making them less flexible in scenarios with incomplete or noisy data. Thus, despite its advantages over RBC, its practical deployment remains constrained by computational and data-related barriers [25].

Deep reinforcement learning (DRL) has emerged as a revolutionary approach to optimizing HP control in DH systems, addressing many of the limitations inherent in traditional strategies [26]. Unlike MPC, which relies on predefined models, DRL learns optimal control policies through interaction with the system environment, allowing it to adapt to varying conditions and uncertainties [27]. DRL's ability to handle high-dimensional state spaces and partial observability makes it particularly suited for complex DH applications.Furthermore, by employing neural networks for decision-making, DRL frameworks can dynamically adjust to real-time data, ensuring both system reliability and performance optimization [28].

In building-level applications, DRL has demonstrated potential for optimizing indoor temperature control and reducing heating energy consumption, with energy savings of 5–12 % reported compared to conventional control methods [29]. Similarly, DRL approaches have been applied to control a set of rooms heated by the district network, showing improvements in both thermal comfort and energy cost reduction compared to baseline strategies [30].

Recent advancements in the design and control of DHS focus mainly on enhancing efficiency, reducing costs, and minimizing the environmental impact. Chan [31] introduced an Genetic Algorithm (GA) for optimizing the piping network of DHS, refining the search

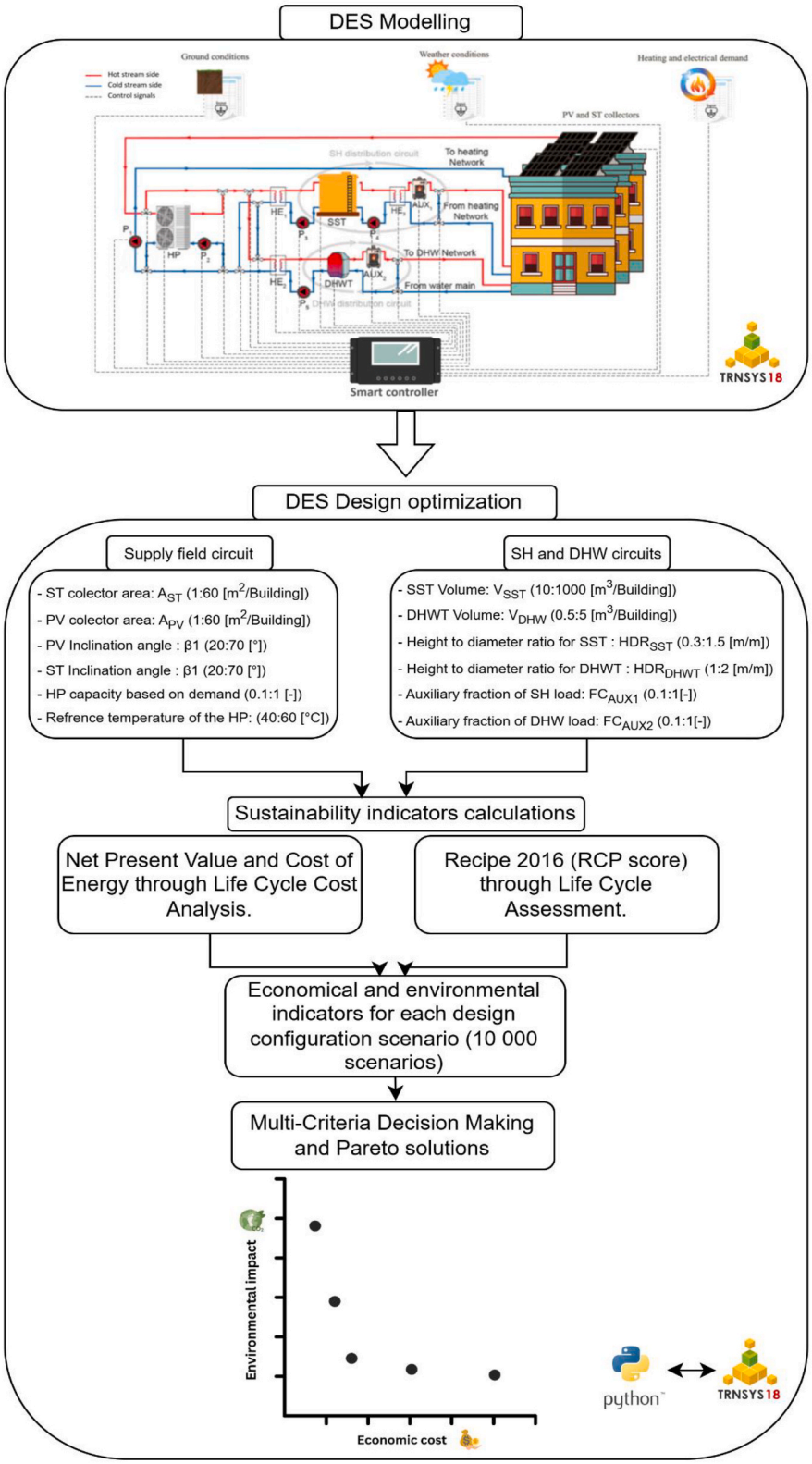

Fig. 1. TRNSYS-Python co-simulation framework for optimizing the DES design.

for optimal configurations by introducing a neighboring search method when local minima are detected. Arslan et al. [32]optimized a geothermal district heating system with thermal energy storage and heat pumps, achieving a 38 % reduction in relative exergoeconomic cost and a 19 % decrease in relative exergoenvironmental impact. The system's energy and exergy efficiencies were 74 % and 19 %, respectively. Arslan et al. [33] developed a novel multistage, multilevel artificial neural network model to optimize a geothermal heat pump-aided district heating system. To achieve optimal design parameters, the model utilized back-propagation learning algorithms, including Levenberg-Marquardt, Pola-Ribiere Conjugate Gradient, and Scaled Conjugate Gradient. The results indicated that the maximum error rate occurred in Pump 2 at 3.0092 %, while the minimum error was observed in the system's coefficient of performance at 0.0018 %. Further, Arslan et al. [34] introduced a hybrid modeling approach for multi-criteria decision-making in energy systems, applying it to a geothermal DHS. Their optimal design achieved an exergy efficiency of 20.25 %, a sustainability index of 1.25, and an NPV of $4.44 million, highlighting the model's effectiveness in balancing economic and environmental objectives. Zhong et al. [35] employed granularity analysis for solar energy integration in DHS, using hierarchical clustering and pipeline optimization. Yang et al. [36] introduced a bi-level optimal configuration model for integrating renewable electricity-based heating in DHS substations, the findings show that during the heating season, the proposed strategy lowers operating and environmental benefit costs by 13.31 % and 5.35 %, respectively. Golmohamadi et al. [37] proposes an Economic MPC that optimizes heat demand in residential buildings within a DHS to minimize energy consumption costs while integrating thermal inertia for flexibility.

Abugabbara et al. [38] provide a bibliographic analysis of the recent advancements in modeling and co-simulating DHS; the analysis shows that coupled simulation between district and building energy models is a novel research area and can benefit in reducing oversizing energy systems. In addition, the analysis demonstrates that the DHS requires advanced control strategies. Kuntuarova et al. [39] conducted a systematic review of available DH network modeling and simulation tools, comparing their modeling approaches, application scope, and functional capabilities. Current DHS studies primarily rely on monolithic, case-specific simulation frameworks. While some research explores the benefits of co-simulation, significant gaps remain. Mazzarino et al. [40] Proposed a modular co-simulation platform to implement the demand side management to reduce the thermal peak arising in the morning due to the attenuation/shutdown of the heating systems during the night, which is typical in Mediterranean regions and negatively affects the performance of the entire production system. Hardy et al. [8] have developed HELICS, a co-simulation platform that enables multi-domain modeling and analysis of power systems, incorporating tools from domains such as electrical power grid, natural gas, transportation, and communications. A hybrid multi-model co-simulation infrastructure that integrates software and hardware simulators to test and evaluate Distributed Energy Resources scenarios effectively is presented in Ref. [41]. Nageler et al. [42] propose a scalable DH simulation framework but exclude thermal storage. Vesaoja et al. [43] integrate control and physical aspects within DH networks but lack a generalized approach and renewable integration.

One of the main challenges in DHS modeling is fully representing complex system behavior, particularly when integrating renewable energy sources such as photovoltaic panels, solar thermal collectors, and heat pumps. Their interactions with thermal energy storage, including seasonal thermal storage and domestic hot water tanks, further complicate system optimization. A holistic co-simulation framework is needed to optimize the design and smart control of renewable energy-based DHS while balancing technical, environmental, and economic factors. To address these gaps, this study proposes a co-simulation framework that enables dynamic system simulations to optimize DHS design and control. The framework integrates multi-objective optimization and multi-criteria decision-making to minimize life cycle costs and environmental impact. The testbed configuration includes various on-site renewables and thermal storage solutions, incorporating DRL and RBC heat pump optimization strategies, providing a comprehensive comparative analysis from technical, environmental, and economic perspectives.

The structure of the paper is organized as follows: Section II outlines the proposed methodology. Sections III and IV detail the case study, results, and discussions, respectively. Section V concludes the paper (see Fig. 1).

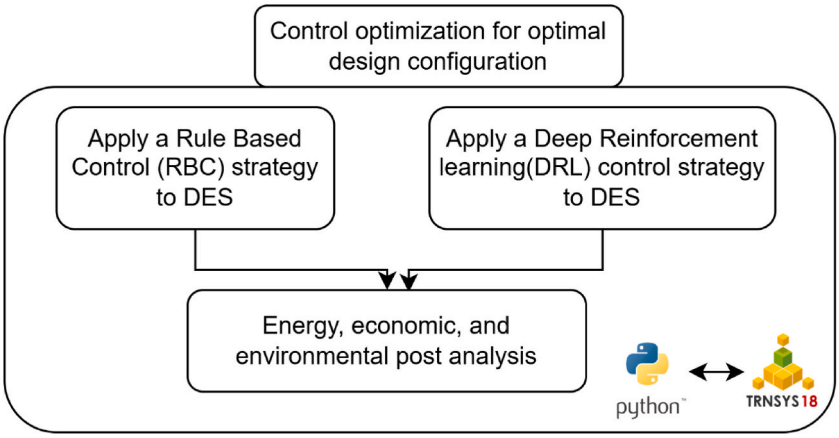

Fig. 2. TRNSYS-Python co-simulation framework for optimizing the DES.

2. Methodology

This section provides a detailed explanation of the methodology used for system modeling, design, and control optimization. Figs. 2 and 3 illustrates the proposed methodological framework, which consists of four main phases. The first phase involves the development of a model for the DES. The second phase focuses on optimizing the design of the DES by minimizing both environmental and economic indicators across 10,000 different configuration scenarios through multi-objective optimizations. A multi-criteria decision-making TOPSIS approach is then used to identify the optimized system design configuration. In the third phase, two control strategies were developed for a water-to-water HP integrated into the DES. The goal is to minimize operational costs and reduce auxiliary natural gas consumption. The final phase includes an analysis of the energy performance, economic, and environmental indicators for each control strategy.

The proposed methodology centers around energy modeling, a foundational concept in renewable energy systems, essential for understanding and optimizing energy processes. This was achieved using the Transient System Simulation Tool (TRNSYS) integrated with Python. The integration utilized Python's subprocess library to transfer necessary variables to TRNSYS and perform simulations. This approach enabled the exploration of diverse system configurations, overcoming geographical constraints and accommodating varied system characteristics, thereby facilitating effective solutions for renewable energy systems.

TRNSYS 18 operates by solving partial differential equations for mass and energy balances within predefined boundaries. However, it has notable limitations in developing and optimizing advanced energy system control algorithms. For instance, implementing smart control methods, such as DRL based approaches, inconvenient and difficult to use directly in the built-in software [44]. To address this, a co-simulation testbed was developed, integrating a DES TRNSYS model with a DRL-based control system to enable dynamic data transfer and interaction between the two, as illustrated in Fig. 2.

The integration of the TRNSYS model with Python is conducted in two main stages, ensuring a seamless data exchange to optimize the system design and control. In the first stage (i.e., system design optimization), TRNSYS sends all system design variables to Python for optimization during each simulation time step. This process leverages the "subprocess" Python library [45] to facilitate communication, allowing the necessary variables to be passed efficiently to TRNSYS for simulation. The second stage of data exchange (i.e., control optimization) occurs at each time step of the TRNSYS simulation, where Python receives inputs from TRNSYS. This is accomplished using the "Calling Python (CFFI)" component, which invokes a Python module located in the same directory as the TRNSYS input file (the deck file). This script can utilize any installed Python package or library, enhancing flexibility and functionality. Communication between TRNSYS (implemented in Fortran) and Python is managed through a Foreign Function Interface using the CFFI Python package [46]. Based on the inputs from TRNSYS, Python then sends control signals back to TRNSYS, completing the feedback loop necessary for real-time simulation adjustments.

Given that DRL training requires extensive simulation data, parallel processing was employed to maximize computational resource efficiency and reduce experimentation time. A Python-based Gym environment [47] was developed to facilitate this, leveraging TRNSYS for parallel simulation data generation.

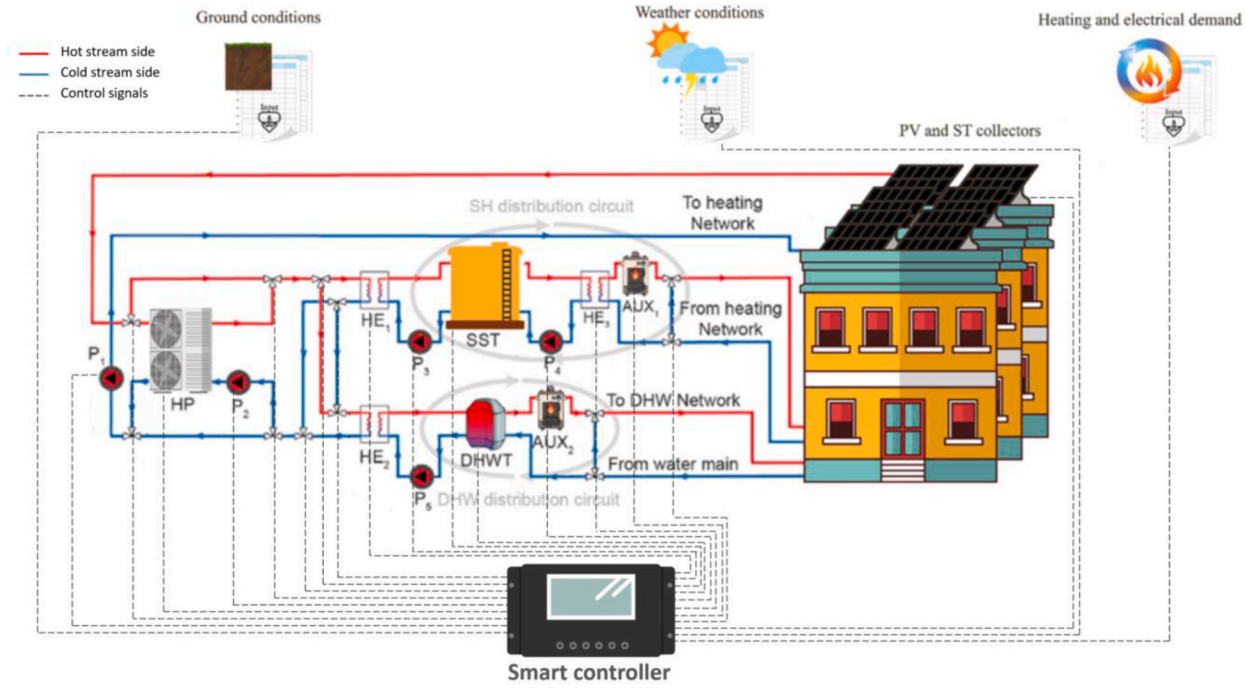

Fig. 3. District energy system DES descriptions.

2.1. Energy system description

An overview of the analyzed DES system, which was developed in the TRYSYS 18 software, is presented in the schematic in Fig. 3. This software uses partial differential equations and imposes constraints on mass and energy conservation under specified boundary conditions. The system's dynamic characteristics were well-captured thanks to the software's ability to simulate the DES realistically. For computational efficiency, the DES model was simulated for three consecutive years. The results of these simulations were then extended across the project's entire lifespan, which was assumed to be 40 years, based on the assumption that weather conditions and demand profiles would remain consistent during this period. The main components of the system are solar thermal (ST) collectors, photovoltaic collectors (PV), the DHW storage tank (DHWT), a half-buried sensible seasonal storage tank (SST), an auxiliary natural gas heater (AUX), and a water-to-water heat pump unit (HP).

As seen in Fig. 2, the HP functions as a heat source for the SST when connected with the solar field circuit. In this arrangement, the space heating (SH) and/or domestic hot water (DHW) demand can be accomplished efficiently by the thermal energy collected from the STC or it can be stored in the SST. An adequate design of the HP that is incorporated in DES is required to meet the SH and DHW needs of a residential community throughout the year. The thermal energy from the solar collectors is transferred to the DHWT in the DHW operation mode, with the intervention of pumps P1, P2, and P5, through HEs and using the 'Y' valves. Meanwhile, the HP unit would be inactive while the DHW mode is activated. In the SH operation mode, heat is transferred from ST to SST through HE1 using pumps P1, P2, and P3, and 'Y' valves. The heat generated by the HP is either provided to the SST for charging up the heat stored or delivered directly to the SH. While the daily DHW demand is supplied by the short-term storage DHWT, the SH demand is supplied only throughout the winter by the SST. The HP operation has two control strategies:

RBC – Here, the HP activates when the average temperature of the SST (T_{SST}) falls below a predefined reference temperature (T_{ref}). This setup serves as the base case scenario.

DRL – In this advanced control strategy, the HP is managed using a model-free strategy that relies on temperature readings from the solar collector (T_{COL}), and the Seasonal Storage Tank (T_{SST}), as well as the set reference temperature (T_{ref}). This approach aims to enhance the system's efficiency by minimizing fluctuations in comfort levels within the SH and DHW systems. Additionally, it focuses on reducing operational costs and limiting the use of auxiliary energy over the course of 3 years. The strategy capitalizes on the adaptive learning capabilities of a DRL algorithm to continuously refine and optimize HP operation based on real-time data and performance outcomes.

In these modes of operation, the heat generated by the HP in controls RBC and DRL will be transferred to either the SST or the DHWT based on demand. In case of insufficient supply for SST or DHWT, the auxiliary heater will be activated as a backup. SH is supplied at a low temperature (50 °C), whereas DHW is supplied at a higher temperature (60 °C). If solar collectors, HP, and SST cannot satisfy the heat load, AUXs cover the shortfall. Additionally, electricity is provided by a combination of on-grid roof-mounted PV panels and the electricity grid, meeting the neighborhood's electric demand and DES electric equipment.

2.2. Economic indicator

In this study, the Life Cycle Costing (LCC) approach was used to economically assess a novel co-simulation framework to optimize a DES. The LCC method takes a future cost perspective and calculates the current value of all expenses incurred over the system's 40-year operational lifespan by applying a discount rate [48]. This includes the initial investment costs (IIC), ongoing operational expenses (OC), and the comprehensive costs of equipment replacement (RC) to determine the net present cost (NPC) [49].

$$NPC = IIC + OC + RC \tag{1}$$

The initial capital cost encapsulates the outset financial investment for the project, covering equipment purchase, installation, transportation, and all other contingency expenses [44]:

$$IIC = (1 + \alpha_{CF}) + \sum_{K} (PCE_K . BMF_K) \tag{2}$$

in equation (2), PCE_k refers to the initial cost of purchasing equipment unit k, BMF_k represents the bare module factor accounting for installation and transportation costs, and α_{CF} is the contingency fee factor. The PCE_k value is adjusted to its present value from the base year (year A) to the installation year (year B) using the Chemical Engineering Plant Cost Index (CEPCI) [44].

$$PCE_K = PCE_K^{year\ A} \frac{CEPCI^{year\ B}}{CEPCI^{year\ A}} \quad \forall k \tag{3}$$

The initial purchase cost for each unit at year A was determined using the following equations [48]:

$$PCE_k^{yearA} = \alpha_k DVE_k^{\beta_k} \quad \forall k = COL, DHW, AUX, PV, HP \tag{4}$$

$$PCE_k^{yearA} = DVE_k^{\beta_k} . 10^{\left[\alpha_k \left(log_{10} DVE_k\right)^{\beta_k}\right]} \quad \forall k = HE_1, HE_2, HE_3 \tag{5}$$

$$PCE_k^{yearA} = \alpha_k \ ln\left(\frac{DVE_k}{1000}\right) + \beta_k \quad \forall k = P_1, P_2, P_3, P_4 \tag{6}$$

$$PCE_k^{yearA} = Ins_{SST} + Con_{SST} \quad \forall k = SST \tag{7}$$

$$\text{Where : } Ins_{SST} = \alpha_k DVE_k^{\beta_k} \quad \forall k = XPS, MW, FG \tag{8}$$

$$Con_{SST} = \alpha_k DVE_k^{\beta_k} \quad \forall k = NC, HPC \tag{9}$$

$$Con_{SST} = \alpha_k e^{\left(\frac{\beta_k}{10^5} DVE_k\right)} \quad \forall k = UHPC \tag{10}$$

Here α_k and β_k represent the parameters for purchasing cost of equipment or materials, DVE_k is the design variables of equipment k. The design variables are the solar collector field area (A_{COL}), the storage tank volume (V_{SST}, V_{DHW}), the SST insulation type (XPS, MW, FG) indicating extruded polystyrene, mineral wool, and foam glass gravel) and its construction materials $NC, HPC, UHPC$ comprising normal concrete, high performance concrete, and ultra-high performance concrete, respectively, along with the HP the heat exchanger areas (HE_1, HE_2, HE_3), and the pumps discharge mass flow rates ($\dot{m}_1$, $\dot{m}_2$, $\dot{m}_3, \dot{m}_4$).

The operational cost (OC) includes yearly maintenance costs for different types of equipment, along with expenses related to electricity consumption and the use of auxiliary natural gas heaters, structured as follows [50]:

$$OC = PW_M + PW_P + PW_{AUX} + PW_{HP} \tag{11}$$

in equation (16), PW_M, PW_{app}, PW_{AUX} and PW_{HP} represent the annual maintenance cost, electricity purchased from the grid, natural gas consumption, and HP electricity consumption cost respectively.

The replacement cost can be calculated using the following formula, which factors in the present value of the equipment [44]:

$$RC = PVF_n \sum_K (PCE_K . BMF_K) \tag{12}$$

Where PVF_n is the present value factor of future cash flow at year n.

2.3. Environmental impact indicators

In conjunction with the Life Cycle Costing (LCC) methodology, which assesses the economic viability of DES, the environmental impacts of the DES systems are evaluated through Life Cycle Assessment (LCA). The LCA methodology provides a comprehensive evaluation of the entire lifecycle of a product or system, from its production to its disposal. This approach follows the "cradle-to-grave" principle,which means that every stage of the product's lifecycle is taken into account. According to the ISO14040 standards [49] standardizes the LCA process, which includes four main phases: goal and scope definition, inventory analysis, impact assessment, and interpretation [51].

For this study, the initial phase of LCA establishes the system boundary and functional unit, adopting a "cradle to gate" perspective that omits the end-of-life disposal phase. This approach is typical in LCA studies, where the disposal phase's impact is often considered minimal relative to the production and usage phases. Similarly, the recycling phase is not emphasized due to its complexity and the challenges associated with accurate forecasting. During the life cycle inventory and impact assessment phase, data on material inputs and outputs, along with associated energy consumption, are collected from various databases for the duration of the system's construction and operation. This analysis included the manufacturing impacts of equipment and the DES's consumption of utilities such as natural gas and electricity over its entire lifetime. Additionally, the transportation of materials to the construction site and the operational impact of system components are evaluated, with impact data sourced from the Ecoinvent 3.9.1 database [52].

The gathered inventory data are then classified into various impact categories, such as human health, ecological systems, and resource depletion. This study employs the ReCiPe 2016 framework, which uses the aggregated endpoint indicator metric (RCP) instead of midpoint indicators. This approach helps avoid potential misinterpretations of the DES's environmental performance, especially when comparing systems of different sizes. The RCP calculations are defined as follows [53]:

$$RCP = \sum_d \delta_d \varepsilon_f FID_d \quad \forall d \tag{13}$$

Where FID_d denotes the final impact of the damage category d, and δ_d, represent the specific normalization and weighting factors. The weighting factors are derived from guidelines provided in the ReCiPe 2016 framework [48].

3. Case study

The small residential community of Falset (41°08′46″N 0°49′12″E), located in the Tarragona province of Spain, was chosen to apply the proposed DES concept. The energy community comprises 1058 buildings with 1712 individual dwellings. The proposed system has been developed to meet the requirements for SH at 50°C, DHW at 60°C, and to fulfill the electricity demand as well.

3.1. Climate and demand profiles

The cluster types of residential buildings in Falset were identified to compute the SH demand using cadastral records [52]. Energy demand estimates per 100 m^2 for each cluster type within Tarragona province were gathered from Ref. [54]. The hourly SH demand was determined by evaluating the difference in temperature between the hourly outdoor air temperature and a constant indoor temperature of 18 °C during the typical heating season (October–May 2023). The meteorological data used for these calculations was a location-specific TMY file from the Photovoltaic Geographical Information System (PVGIS) platform [55]. The hourly SH demand was determined by dividing the annual total according to the temperature difference for each hour.

For DHW, the residential sector's hourly fractional demand was established, as shown in Table 1, with the daily and hourly tap water supply temperatures T_w calculated accordingly.

The formula for the daily DHW energy demand $Q_{DHW}(J)$ for the municipality is defined as [48]:

$$Q_{DHW} = P \,.\, V \,.\, \rho \,.\, C \,.\, \left(T_{sup} - T_w\right) \tag{14}$$

Where P is the municipality's population, V is the recommended volume per person per day, 0.03 m^3 [55] ρ , C, T_{sup} and , T_w are the density of water in (kg/m^3), the specific heat capacity of water (J/kg°C), the supply temperature of hot water, and the tap water temperature, °C, respectively.

A Python-based script was used to gather the hourly electrical consumption data for Falset via the Datadis platform [56].

Fig. 4 shows the monthly DHW, SH, and electricity demand for a neighborhood in Falset that consists of 1058 residential buildings. Each building is equipped with a DHW system and radiant underfloor heating system to meet the requirement for SH and DHW at 50 °C and 60 °C, respectively. Each building requires yearly 1514 kWh, 11425 kWh, and 3989 kWh of domestic heating water, SH, and electricity consumption, respectively (see Fig. 5).

3.2. Economic and environmental input data

The parameters for the LCC assessment are outlined in Table 2. Based on [57], the maintenance cost is estimated to be 1.5 % of the initial purchase cost of the equipment. According to the EUROSTAT database [58], natural gas and electricity prices are 0.0862 Euro/kWh and 0.2871 Euro/kWh, respectively. The price of electricity injected into the grid is 0.10 Euro/kWh [59]. In addition, the inflation rate associated with natural gas and electricity is 5.6 % and 3.9 %, respectively. The inflation rate associated with the proposed system throughout its lifetime was set to be 1.61 %, with a discount rate of 0.64 % [57]. The detailed parameters for the initial investment are presented in Table 2.

The input parameters for the LCA were selected from the Ecoinvent v. 3.9.1 database [52]. It categorizes the damage associated with the DES components based on the Recipe 2016 approach. The cumulative endpoint environmental impact is calculated with Equation (13) and the specific impact of different components of the DES is shown in Table 3.

4. Results and discussion

This study organizes its findings into three sections: the first examines optimal design configurations of the DES through multi-objective optimization and multi-criteria decision-making using TOPSIS; the second evaluates thermal energy performance with two control strategies in a residential community of 1058 buildings in Falset, addressing demands for SH, DHW, and electricity; the third section assesses LCC and environmental impacts of the optimal design, integrating various control strategies.

Fig. 6 presents an optimum system design of the DES, illustrating the trade-offs between Specific Economic Cost (SEC) (€/MWh) and environmental impacts - RCP (Pt/MWh) across various design scenarios. The Pareto front presented in the plot highlights the balance between minimizing costs and reducing environmental impacts, with data ranging from €29.87 to €65 per MWh for specific economic costs and from 3.4 to 5.8 Pt/MWh for environmental impacts. Notably, the minimal cost solution is 29.87 Euro/MWh with an environmental impact of 5.8 Pt/MWh. In contrast, the minimal RCP solution presents an RCP of 3.4 Pt/MWh at a significantly higher SEC of €65 per MWh. When comparing the minimal cost solution to the minimal RCP solution, there is a substantial increase of

Table 1
The hourly fractional DHW demand.

Hour	f_h	Hour	f_h	Hour	f_h
0h	0.01	8h	0.07	16h	0.04
1h	0.00	9h	0.07	17h	0.04
2h	0.00	10h	0.06	18h	0.05
3h	0.00	11h	0.06	19h	0.07
4h	0.00	12h	0.05	20h	0.06
5h	0.01	13h	0.05	21h	0.06
6h	0.03	14h	0.04	22h	0.05
7h	0.01	15h	0.03	23h	0.05

* f_h refers to the fraction concerning the daily total DHW demand.

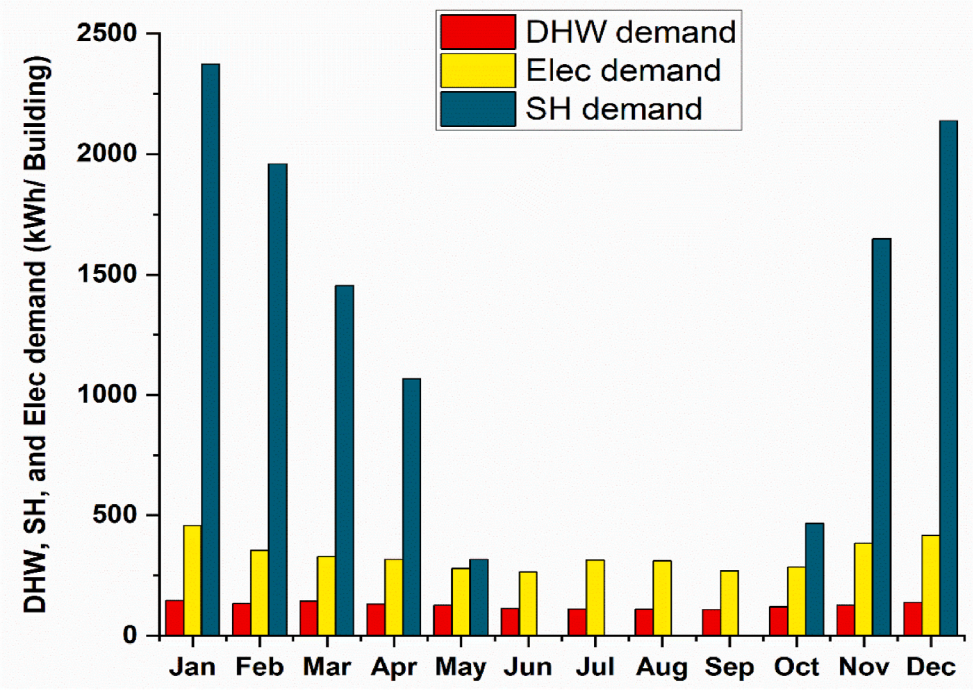

Fig. 4. Demand profiles for DHW, SH and electricity per month for the investigated energy community of Falset.

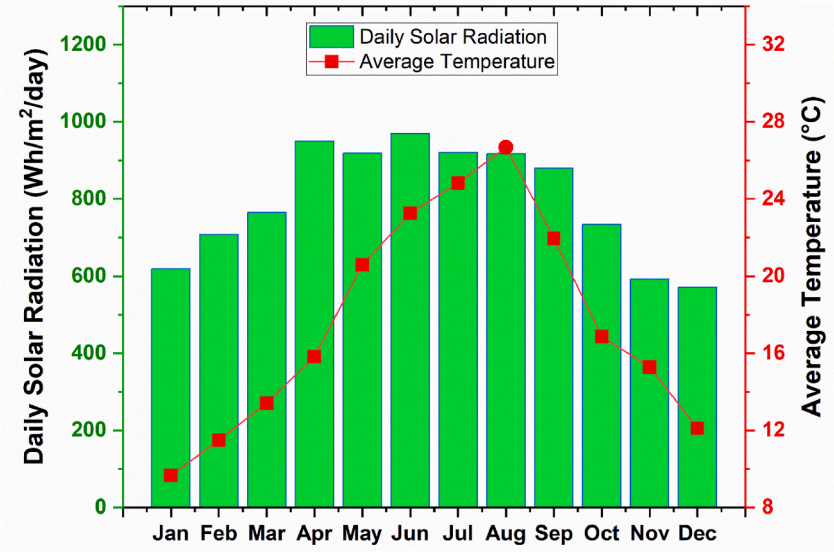

Fig. 5. The monthly climatic conditions of the investigated energy community of Falset.

approximately 116 % in SEC when moving from the minimum SEC solution at €29.87 to the minimum RCP solution at €65. Simultaneously, there is a significant decrease in environmental impact by about 41 % from 5.8 Pt/MWh to 3.4 Pt/MWh. The balanced solutions, which aim to give equal weight to economic cost and environmental impact, are particularly intriguing. This solution is €34 per MWh for SEC and exhibits RCP values between 4.6 Pt/MWh. They represent a practical middle ground, with about a 13.8 % increase in SEC and a decrease in RCP of 20.7 % compared to the minimal-cost solutions.

Fig. 7 provides a detailed analysis of the optimal system design for DES, focusing on four main decision variables: PV area, STC area, SST volume, and DHWT volume. Each box represents the optimal size range for these components, with whiskers indicating the optimization boundaries and the solid box defining the interquartile range, highlighting the most likely values. From the optimization results, different system design approaches emerge based on cost, balance, and environmental impact. The **minimum cost solution**

Table 2
The economic parameters of DES equipment.

Equipment, material	*Options*	α_k	β_k	DEV_k	Base year	BMF_k	*Ref.*
STC		974.2	0.8330	Aperture area (m^2)	2007	1.00	[20]
PV		190.92	0.833	Aperture area (m^2)	2022	1.00	
HP		2053.8	−0.348	Capacity(kW)		1.40	
DHWT		3955	0.6500	Volume (m^3)	2007	1.00	[21]
Aux		225.0	0.7460	Duty (kW)	2001	2.10	[22]
HE		3.133	0.3310	Exchange area (m^2)	2001	3.29	[22]
Pump (P_1, P_2)		389.0	283.2	Mass flow rate (kg/h)	2009	3.24	[23]
Pump (P_3, P_4)		389.0	717.0	Mass flow rate (kg/h)	2009	3.24	[23]
SST insulation	*XPS*	561.09	0.397	Material thickness (m)	2017	1.00	[24]
	MW	1902.7	0.942	Material thickness (m)	2018	1.00	[25]
	FG	311.41	0.968	Material thickness (m)	2014	1.00	[26]
STT construction	*NC*	4178.1	−0.394	Volume (m^3)	2000	1.00	
	HPC	2575	−0.363	Volume (m^3)	2004	1.00	[27]
	UHPC	90.83	−3	Volume (m^3)	2004	1.00	

Table 3
The environmental impact of DES equipment based on ReCiPe 2016 [48].

Unit	Option	Impact factor (ReCiPe 2016)
ST		10.17 Pt/m^2
PV		15.70 Pt/m^2
HP		7.052 Pt/kW
DHWT		85.96 Pt/m^3
Auxiliary boiler		4.11 Pt/kW
Heat exchanger		2.515 Pt/m^2
Pump		4.531 Pt/kW
SST insulation	*XPS*	0.889 Pt/kg
	MW	0.0018 Pt/kg
	FG	0.166 Pt/kg
SST construction	*NC*	0.008 Pt/kg
	HPC	0.002 Pt/kg
	UHPC	0.0206 Pt/kg
Natural gas		0.0265 Pt/kWh
Electricity		0.0380 Pt/kWh

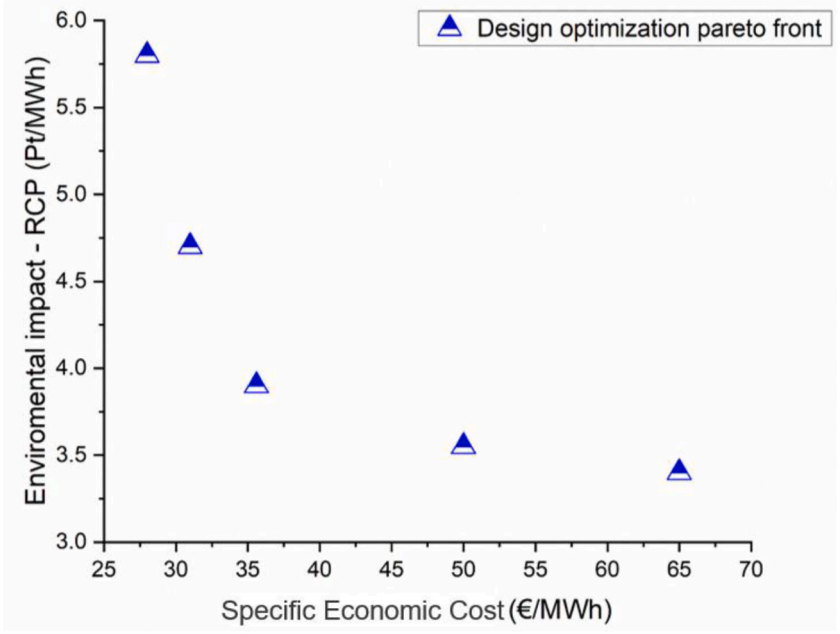

Fig. 6. Multi-objective optimization for optimal scenario selection: Pareto sets analysis.

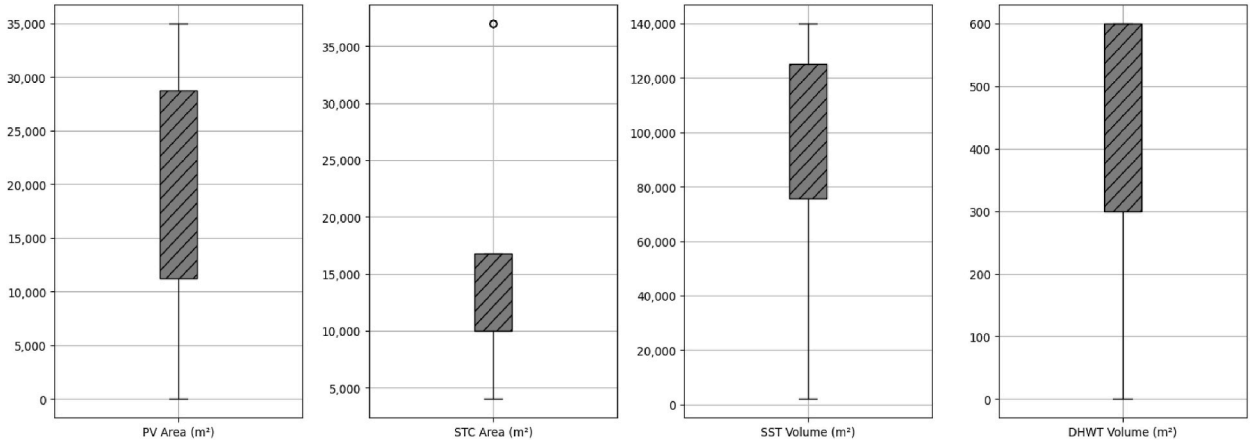

Fig. 7. Optimal system design ranges for district energy system.

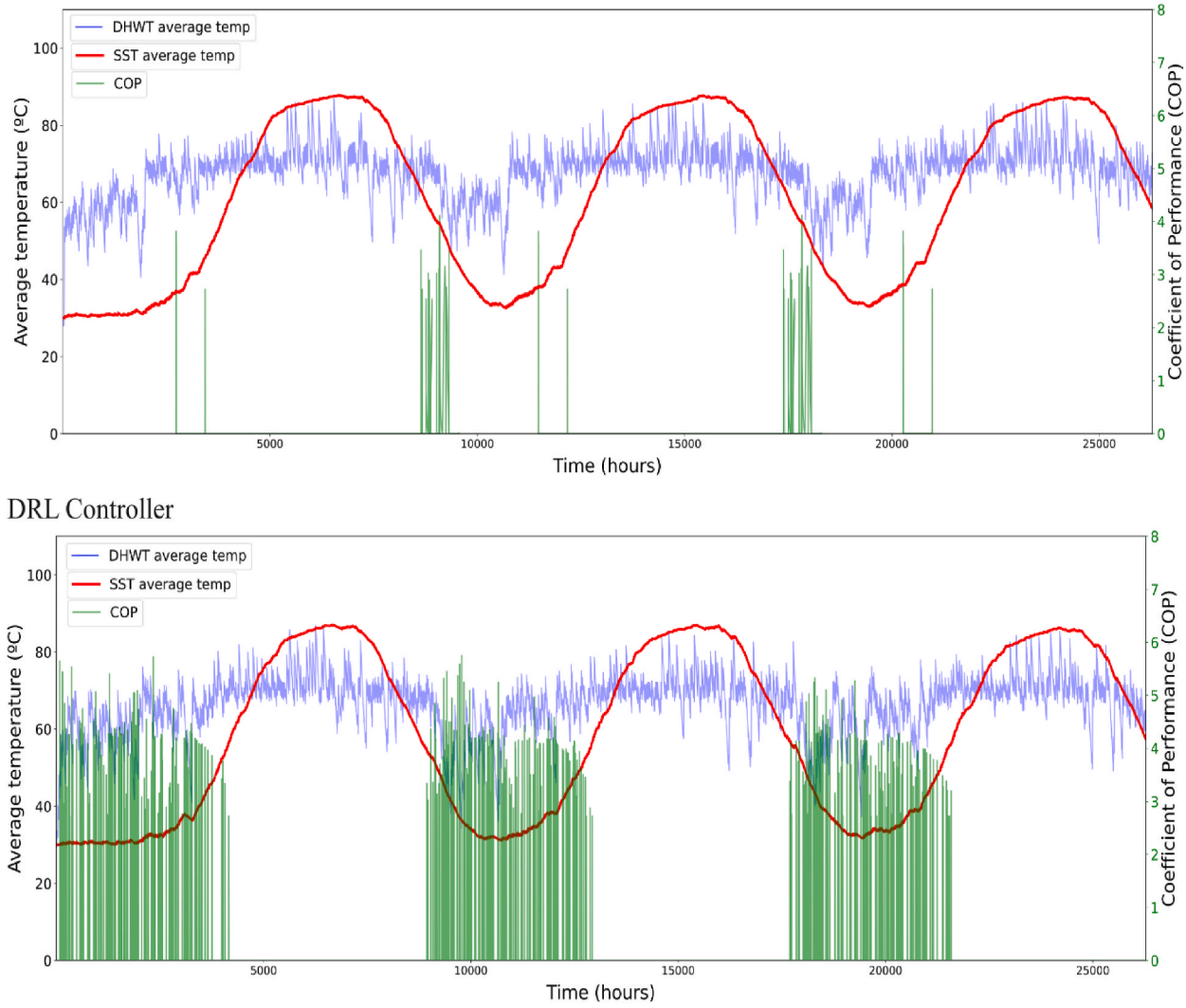

Fig. 8. Operations temperatures of the DHW and seasonal thermal storage tanks and coefficient of performance of the DES under a RBC and DRL controllers.

favors a larger PV area (28,900 m^2) and SST volume (129,826 m^3) to achieve cost efficiency, while maintaining a moderate DHWT volume (605 m^3) and a STC area (10,818 m^2). The balanced solution reduces the PV area to 19,300 m^2 and the SST volume to 108,188 m^3, optimizing trade-offs between cost and sustainability. It also lowers the DHWT volume to 504 m^3, indicating an efficient balance between thermal storage components. The **minimum impact solution** minimizes the PV area to 9700 m^2 and SST volume to 97,369 m^3, prioritizing environmental impact reduction while keeping STC and DHWT volumes unchanged at 10,818 m^2 and 605 m^3, respectively.

After achieving the optimal system design through the Multi-objective optimization, the heating control systems were evaluated, particularly the comparison between a RBC, and DRL controller; the analysis focused on performance over a three-year period, specifically 26,280 h of operation.

Fig. 8 illustrates the average temperatures inside the DHWT in blue, the average temperatures inside the SST in red, and the COP in green for both controllers. By using the DRL controller, the fluctuations in the DHWT temperature seem slightly more subdued

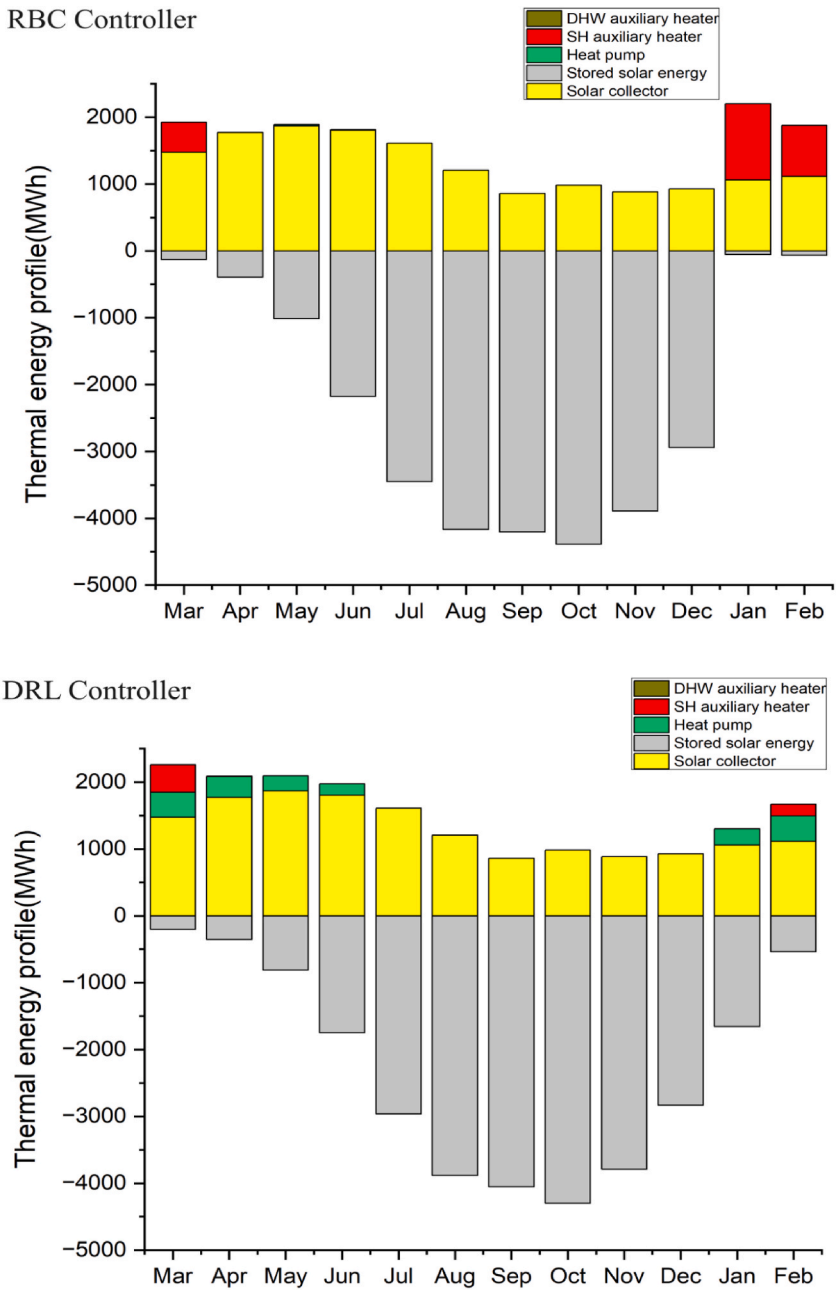

Fig. 9. Comparative analysis of the annual thermal energy management of the optimal system design under RBC and DRL controllers.

compared to the RBC controller; additionally, the DRL controller demonstrated a higher consistency in DHWT temperature control, adhering closely to set temperatures with minimal deviations (−0.48 K for DHW and −0.51K for SH set temperatures), indicating superior control precision compared to the RBC, which exhibited larger deviations (−2.06 K for DHW and 3.51 K for SH). These deviations signify control accuracy and suggest differences in energy efficiency, as closer adherence to set temperatures generally leads to reduced energy consumption. In the first part of the reward function formulation of the controller's DRL algorithm, the goal was to minimize the comfort deviations for both SH and DHW, which justified why the DRL overperforms the RBC.

In assessing the operational dynamics of the DRL and RBC controllers within the context of system operation t, a critical point of comparison emerges in the functioning and impact of the HP, particularly evident in their respective contributions to the overall COP. This analysis shows that the DRL controller achieves a seasonal COP of 3.95 and a maximum COP of 5.71, with the HP contributing approximately 17 % to the total heating demand. In contrast, the RBC controller achieves a lower seasonal COP of 3.29 and a maximum COP of 4.42, with a minimal HP contribution of only 1 %. The higher COP values and significant HP contribution under the DRL controller indicate a more active engagement of the HP in thermal energy management. This suggests a strategic use of the HP to enhance system efficiency, an approach that not only improves overall energy efficiency but also ensures that the HP is utilized to maximize its potential benefits and reduce reliance on natural gas auxiliary heaters. Conversely, the strategy employed by the RBC controller, which results in lower COP values and negligible HP usage, implies a potentially underutilized capacity of the HP, leading to less efficient system operation.

Fig. 9 illustrates a comparative analysis of the annual thermal energy management under RBC and DRL controllers within the DES. The figure showcases the monthly energy contributions from the various components including the solar collectors, stored solar energy, HP, and auxiliary heaters. Notably, energy stored in the SST from February to September is depicted as negative in grey, indicating periods of energy accumulation rather than usage. This stored energy is then utilized during autumn and early winter, demonstrating the system's ability to effectively balance supply and demand. The thermal energy provided by the solar collectors, SH auxiliary heater, and HP are presented in yellow, red, and green colors, respectively.

The RBC shows marked seasonal fluctuations, especially in the coldest months, heavily relying on stored energy and auxiliary heating due to minimal HP contribution, less than 1 %. In contrast, the DRL controller manages a more efficient and stable energy output, significantly incorporating the HP throughout the year, accounting for approximately 17 % of the energy consumption profile. This optimized strategy enhances the HP's seasonal performance, reduces the need for auxiliary heating, and stabilizes the SST's temperature and internal energy change.The DRL controller provides a balanced and integrated approach to managing the heat sources, including solar collectors, storage tanks, HPs, and auxiliary heaters, ensuring reliable and efficient heating for 1058 residential buildings in Falset, Spain. The enhanced control strategy of the DRL not only optimizes energy utilization but also maintains consistent service levels, showcasing its superiority over traditional RBC systems in complex heating operations. This analysis highlights the benefits of implementing advanced DRL techniques for energy management in DH systems, promoting sustainability and operational efficiency.

Fig. 10 provides a comparative analysis of solar fraction and efficiency metrics across different components of an DES, controlled by either a RBC or a DRL controller. The figure is segmented into two primary categories: Solar Fraction (SF) and Efficiency, each further divided into subcategories for SH, DHW, and solar collectors. The metrics demonstrate the DRL controller's superior performance in harnessing solar energy, with a global solar fraction of 87.98 % compared to the RBC's 77.26 %. This enhanced performance extends to SH, where the DRL achieves an 86.80 % solar fraction compared to the RBC's 74.81 %. Both controllers show high system's efficiency in the provision of DHW, with the DRL slightly outperforming the RBC (96.84 % vs. 95.74 %). In terms of efficiency, the DRL controller exhibits improved collector efficiency at 80.47 %, against the RBC's 77.63 %, indicating more effective solar energy conversion. SH efficiency is slightly higher under the RBC at 97.15 %, compared to 96.77 % for the DRL, a marginal difference that might reflect specific operational strategies of the RBC. Both controllers achieve nearly identical high efficiencies in DHW heating at 99.80 %.

Table 4 presents a life cycle costing comparison for an optimal design solution of an integrated HP into a DES, employing two distinct control strategies: RBC and DRL. The table details various cost aspects, including initial capital costs, replacement costs, operation and maintenance costs, NPC, and the economic cost per megawatt-hour. We used the same optimal system design, resulting in identical initial capital and replacement costs of €7.22 million and €2.74 million, respectively. This ensures that operational efficiency differences stem solely from the controllers' management strategies, not system design variations.

The DRL controller significantly reduces operational and maintenance costs to €9.81 million compared to €13.22 million for the RBC, primarily due to its optimized utilization of the HP. This efficient management leads to a lower NPC of €19.77 million for DRL, against €23.18 million for RBC, and reduces the economic cost per MWh to €34.01, compared to €35.53 under RBC. Furthermore, as highlighted in Figs. 7 and 8, the DRL's strategic advantage in maximizing HP usage significantly contributes to the system's energy profile throughout the year and minimizes auxiliary heater reliance. In contrast, the RBC exhibits high dependence on auxiliary heaters due to underutilization of the HP, resulting in increased operational costs.

Fig. 11 presents a detailed comparison of the environmental impact of the optimal design solution under RBC and DRL control strategies of an integrated HP into DES. The environmental impact of electricity usage, denoted as Impact_e, is slightly higher for the DRL at 2.12 Pt/MWh compared to 2.02 Pt/MWh for the RBC. This indicates a potentially higher electricity consumption under the DRL, suggesting that the DRL engages the HP more actively, as illustrated in green color in Fig. 6. Both controllers demonstrate identical impacts from solar collector (Impact_COL), photovoltaic collector (Impact_PV), domestic hot water tanks (Impact_TankDHW), and HP (Impact_HP), this similar impact is due to the same optimal system design. Thermal energy storage (Impact_TTES) shows insightful variations. While the impact from thermal energy storage remains constant between the controllers, the DRL shows a heightened impact from seasonal thermal storage, suggesting a more pronounced utilization of this storage tank, as illustrated in Fig. 9, during the months of January and February. The DRL controller exhibits a 1.56 % decrease in total environmental impact measured in

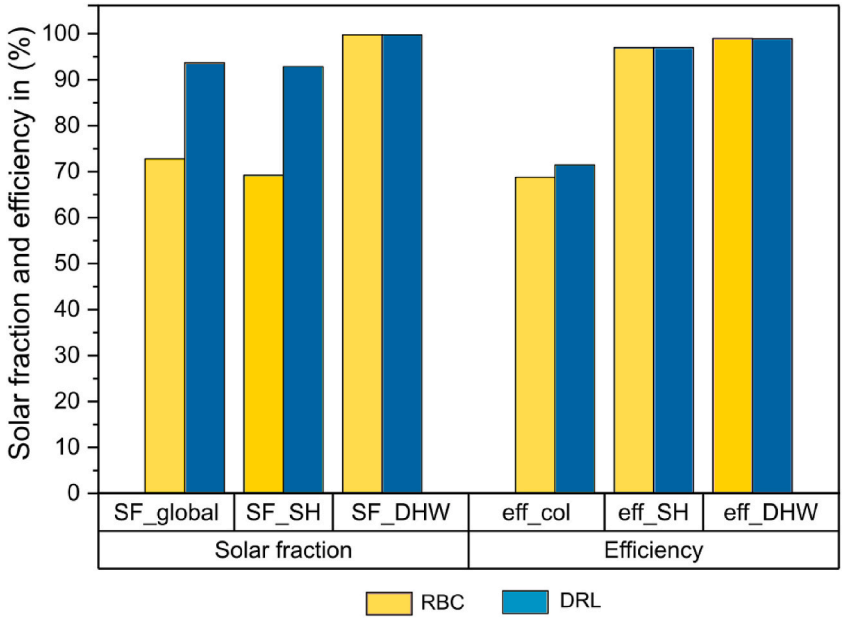

Fig. 10. Solar fraction of the SH, DWH circuits, and efficiency of solar collectors, SH, and DHW under the RBC and DRL controllers.

Table 4
Economic comparison for the optimal design solution under RBC and DRL controllers.

	RBC	DRL
Initial investment cost (M€)	7.22	7.22
Replacement cost (M€)	2.74	2.74
Operation and maintenance cost (M€)	13.22	9.81
Net present cost (M€)	23.18	19.77
Specific economic cost (€/MWh)	35.53	34.01

Pt/MWh compared to the RBC. The DRL controller's reduction in total environmental impact is primarily due to its enhanced operation control of the HP, which is powered by solar energy rather than relying on auxiliary heaters fueled by natural gas.

Overall, the design and control optimization facilitated by the DRL controller has demonstrated an exemplary integration of heat sources—solar collectors, storage tanks, HP, and auxiliary heaters ensuring a reliable and continuous supply of SH and DHW to the residential community of 1058 residential buildings in Falset, Spain. This strategy optimizes energy utilization and significantly enhances the sustainability of the system. The findings clearly highlight the superior performance and efficiency of advanced control strategies like DRL in managing DES, offering benefits from energy, economic, and environmental perspectives.

5. Conclusion

This study provides a comprehensive analysis of optimizing DES through a co-simulation framework developed between TRNSYS and Python. The framework was applied to a medium-sized residential community of Falset municipality of the Tarragona province, Spain. The co-simulation framework contains the dynamic TRNSYS model of the DES, with HP and seasonal thermal storage tank. A Python model was used for the system's design and the smart control optimization as well as the technical, environmental, and economic assessments.

- Through multi-objective optimization and multi-criteria decision-making, we identified optimal configurations that reduce net present cost by 14.71 % and reduce environmental impacts by 11.09 %.
- The optimal system design configuration was found to be a PV area of 19,300 m^2, SST volume of 108,188 m^3, STC area of 10,818 m^2, and DHWT volume of 504 m^3, providing a balanced solution between cost reduction and environmental impact.
- Comparative performance analysis revealed that the DRL controller maintained tighter control over temperature settings, with deviations as minimal as −0.48 K for DHW and −0.51 K for SH; this outperformed the RBC, which showed larger deviations (−2.06 K for DHW and 3.51 K for SH). This precision in temperature management under the DRL controller indicates a higher efficiency and leads to substantial energy savings by minimizing unnecessary heating.

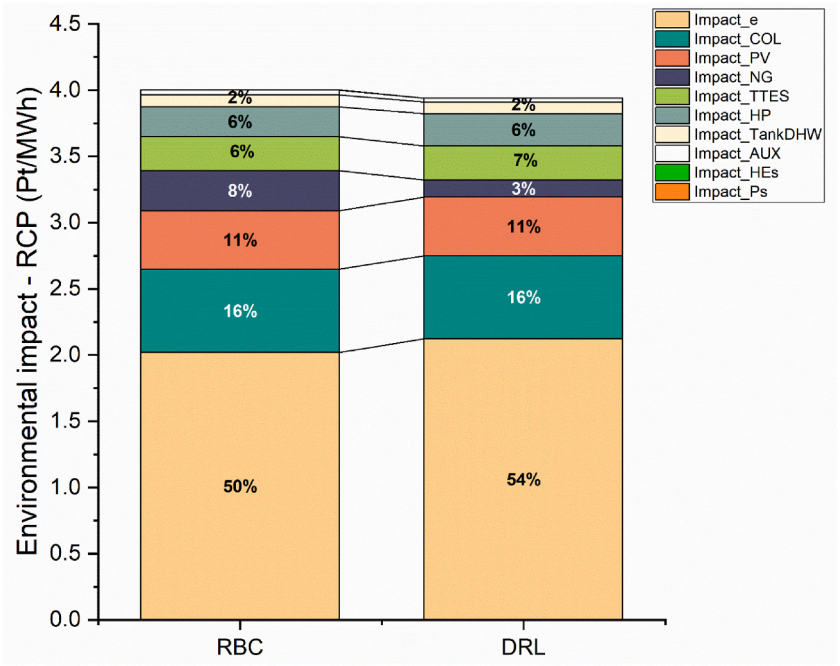

Fig. 11. Environmental impact comparison for the optimal design solution under RBC and DRL controllers.

- The life cycle cost analysis further supports DRL's economic viability, showing annual savings in operations and maintenance costs of approximately €0.08 million and a 4.28 % reduction in economic net present cost.
- Additionally, the DRL approach cuts environmental impacts by 1.56 %, primarily through optimized HP operations reliant on solar energy, thus reducing dependence on auxiliary natural gas heaters. The HP accounts for 17 % of total energy consumption and achieves a global solar fraction of 87.98 %.

These findings highlight the essential role of advanced hybrid co-simulation frameworks in improving DES design and control, emphasizing their potential for sustainable urban energy transitions.

CRediT authorship contribution statement

Youssef Elomari: Writing – original draft, Visualization, Validation, Software, Methodology, Investigation, Formal analysis, Conceptualization. **Giorgos Aspetakis:** Writing – review & editing. **Carles Mateu:** Writing – review & editing, Supervision, Software, Investigation. **Adedamola Shobo:** Writing – review & editing. **Dieter Boer:** Writing – review & editing, Supervision, Resources, Project administration, Funding acquisition. **M. Marín-Genescà:** Writing – review & editing, Supervision, Funding acquisition. **Qian Wang:** Writing – review & editing, Supervision, Resources, Project administration, Funding acquisition.

Declaration of competing interest

The authors declare that they have no known competing financial interests or personal relationships that could have appeared to influence the work reported in this paper.

Acknowledgment

The authors wish to acknowledge financial support from the "Ministerio de Ciencia, Innovación y Universidades" of Spain (PID2021-127713OA-I00, PID2021-123511OB-C31, PID2021-123511OB-C33, PID2021-124139NB-C22 funded by MCIN/AEI/10.13039/501100011033/FEDER, UE & TED2021-129851B-I00 funded by MCIN/AEI/10.13039/501100011033 and "Diputació de Tarragona", 2020PMF-PIPF-29.and by the "European Union NextGenerationEU/PRTR), and "Ministerio de Ciencia, Innovación y Universidades" of Spain through the Recovery, Transformation and Resilience Plan; "The European Union – NextGenerationEU"; and "Universitat Rovira i Virgili" [2021URV-MZ-11], The authors wish to acknowledge the European Union for supporting this work by means of the MULTICLIMACT project (Grant Agreement No. 101123538). The authors gratefully acknowledge the financial support from the Swedish Energy Agency (grant number: 52488–1).

Data availability

Data will be made available on request.

References

[1] L. Pérez-Lombard, J. Ortiz, C. Pout, A review on buildings energy consumption information, Energy Build. 40 (3) (2008) 394–398, https://doi.org/10.1016/j.enbuild.2007.03.007.
[2] G. Cheshire, Directive (EU) 2018/844 of the European Parliament and of the Council of 30 May 2018 Amending Directive 2010/31/EU on the Energy Performance of Buildings and Directive 2012/27/EU on Energy Efficiency, 2011, pp. Vol19:67–Vol19:68. *Dir. 2018/844*, no. November 2010.
[3] S. Werner, International review of district heating and cooling, Energy 137 (2017) 617–631, https://doi.org/10.1016/j.energy.2017.04.045.
[4] C. Energy, S. Report, O.N. Technology, V. Chains, Clean Energy Technology Observatory Status Report On Technology Renewable Fuels Of Non- Biological Origin In the European, 1831, https://doi.org/10.2760/4896278.
[5] H. Li, N. Nord, Transition to the 4th generation district heating - possibilities, bottlenecks, and challenges, Energy Proc. 149 (2018) 483–498, https://doi.org/10.1016/j.egypro.2018.08.213.
[6] H. Lund, et al., 4th Generation District Heating (4GDH). Integrating smart thermal grids into future sustainable energy systems, Energy 68 (2014) 1–11, https://doi.org/10.1016/j.energy.2014.02.089.
[7] M. Lumbreras, R. Garay, Energy & economic assessment of façade-integrated solar thermal systems combined with ultra-low temperature district-heating, Renew. Energy 159 (2020) 1000–1014, https://doi.org/10.1016/j.renene.2020.06.019.
[8] T.D. Hardy, B. Palmintier, P.L. Top, D. Krishnamurthy, J.C. Fuller, HELICS: a Co-simulation framework for scalable multi-domain modeling and analysis, IEEE Access 12 (January) (2024) 24325–24347, https://doi.org/10.1109/ACCESS.2024.3363615.
[9] F. Schloegl, S. Rohjans, S. Lehnhoff, J. Velasquez, C. Steinbrink, P. Palensky, Towards a classification scheme for co-simulation approaches in energy systems. Proc. - 2015 Int. Symp. Smart Electr. Distrib. Syst. Technol. EDST 2015, 2015, pp. 516–521, https://doi.org/10.1109/SEDST.2015.7315262.
[10] R. Yuan, et al., Modelling and Co-simulation of hybrid vehicles: a thermal management perspective, Appl. Therm. Eng. 180 (August) (2020) 115883, https://doi.org/10.1016/j.applthermaleng.2020.115883.
[11] S. Kuntuarova, T. Lickleder, T. Huynh, D. Zinsmeister, T. Hamacher, V. Perić, Design and simulation of district heating networks: a review of modeling approaches and tools, Energy 305 (January) (2024), https://doi.org/10.1016/j.energy.2024.132189.
[12] P. Palensky, E. Widl, M. Stifter, A. Elsheikh, Modeling intelligent energy systems: Co-simulation platform for validating flexible-demand EV charging management, IEEE Trans. Smart Grid 4 (4) (2013) 1939–1947, https://doi.org/10.1109/TSG.2013.2258050.
[13] E. Widl, C. Wild, K. Heussen, E. Rikos, T.T. Hoang, Comparison of two approaches for modeling the thermal domain of multi-energy networks. 1st Int. Work. Open Source Model. Simul. Energy Syst. OSMSES 2022 - Proc., 2022 870620, https://doi.org/10.1109/OSMSES54027.2022.9769129, 1–6.
[14] A. Afram, F. Janabi-Sharifi, Theory and applications of HVAC control systems - a review of model predictive control (MPC), Build. Environ. 72 (2014) 343–355, https://doi.org/10.1016/j.buildenv.2013.11.016.
[15] G. Zsembinszki, V. David, L.F. Cabeza, Deep Learning Optimal Control for a Complex Hybrid Energy Storage System, 2021.
[16] E. Psimopoulos, E. Bee, J. Widén, C. Bales, Techno-economic analysis of control algorithms for an exhaust air heat pump system for detached houses coupled to a photovoltaic system, Appl. Energy 249 (Sep. 2019) 355–367, https://doi.org/10.1016/j.apenergy.2019.04.080.
[17] H. Zhang, D. Wu, B. Boulet, A review of recent advances on reinforcement learning for smart home energy management, in: 2020 IEEE Electric Power and Energy Conference, EPEC 2020, Institute of Electrical and Electronics Engineers Inc., Nov. 2020, https://doi.org/10.1109/EPEC48502.2020.9320042.
[18] M.H. Abokersh, M. Vallès, K. Saikia, L.F. Cabeza, D. Boer, Techno-economic analysis of control strategies for heat pumps integrated into solar district heating systems, J. Energy Storage 42 (2021), https://doi.org/10.1016/j.est.2021.103011.
[19] K. Katsavounis, P. Hou, W. Hu, Z. Chen, Optimized control of a residential heat pump, IEEE PES Innov. Smart Grid Technol. Conf. Eur. ISGT-Europe 2017 - Proc. 2018-Janua (2017) 1–6, https://doi.org/10.1109/ISGTEurope.2017.8260141, 2017.
[20] F. Oldewurtel, et al., Energy efficient building climate control using Stochastic Model Predictive Control and weather predictions, Proc. 2010 Am. Control Conf. ACC 2010 (August) (2010) 5100–5105, https://doi.org/10.1109/acc.2010.5530680.
[21] F. Lie-Jensen, A. Aannø, E. Aleksandrova, A. Westli, M. Nielsen, T. Komulainen, Model predictive control of district heating system, Proc. 59th Conf. imulation Model. (SIMS 59), 26-28 Sept. 2018, Oslo Metrop. Univ. Norw. 153 (September) (2018) 43–50, https://doi.org/10.3384/ecp1815343.
[22] F. Verrilli, et al., Model predictive control-based optimal operations of district heating system with thermal energy storage and flexible loads, IEEE Trans. Autom. Sci. Eng. 14 (2) (2017) 547–557, https://doi.org/10.1109/TASE.2016.2618948.
[23] X. Xin, Z. Zhang, Y. Zhou, Y. Liu, D. Wang, S. Nan, A comprehensive review of predictive control strategies in heating, ventilation, and air-conditioning (HVAC): model-free VS model, J. Build. Eng. 94 (April) (2024) 110013, https://doi.org/10.1016/j.jobe.2024.110013.
[24] T. Wei, Y. Wang, Q. Zhu, Deep reinforcement learning for building HVAC control, in: Proceedings - Design Automation Conference, Institute of Electrical and Electronics Engineers Inc., Jun. 2017, https://doi.org/10.1145/3061639.3062224.
[25] A. Nagy, H. Kazmi, F. Cheaib, and J. Driesen, “Deep Reinforcement Learning for Optimal Control of Space Heating.”.
[26] S. Gupta, G. Singal, D. Garg, Deep reinforcement learning techniques in diversified domains: a survey, Arch. Comput. Methods Eng. 28 (7) (Dec. 2021) 4715–4754, https://doi.org/10.1007/s11831-021-09552-3.
[27] D. Weinberg, Q. Wang, T.O. Timoudas, C. Fischione, A review of reinforcement learning for controlling building energy systems from a computer science perspective, Sustain. Cities Soc. 89 (December 2022) (2023) 104351, https://doi.org/10.1016/j.scs.2022.104351.
[28] J. Deng, et al., Deep reinforcement learning for fuel cost optimization in district heating, Sustain. Cities Soc. 99 (August) (2023), https://doi.org/10.1016/j.scs.2023.104955.
[29] S. Brandi, M.S. Piscitelli, M. Martellacci, A. Capozzoli, Deep reinforcement learning to optimise indoor temperature control and heating energy consumption in buildings, Energy Build. 224 (2020) 110225, https://doi.org/10.1016/j.enbuild.2020.110225.
[30] A. Le-Coz, T. Nabil, F. Courtot, Towards optimal district heating temperature control in China with deep reinforcement learning, NeurIPS 2020 Work. Tackling Clim. Chang. with Mach. Learn. (i) (2020) [Online]. Available: http://arxiv.org/abs/2012.09508.
[31] L.S. Chan, Piping network optimization for district heating system using an enhanced Genetic Algorithm searching method, J. Build. Eng. 95 (March) (2024) 110078, https://doi.org/10.1016/j.jobe.2024.110078.
[32] O. Arslan, A.E. Arslan, I. Kurtbas, Exergoeconomic and exergoenvironmental based multi-criteria optimization of a new geothermal district heating system integrated with thermal energy storage driven heat pump, J. Build. Eng. 73 (April) (2023) 106733, https://doi.org/10.1016/j.jobe.2023.106733.
[33] H. Arat, O. Arslan, Optimization of district heating system aided by geothermal heat pump: a novel multistage with multilevel ANN modelling, Appl. Therm. Eng. 111 (2017) 608–623, https://doi.org/10.1016/j.applthermaleng.2016.09.150.
[34] A.E. Arslan, O. Arslan, M.S. Genc, Hybrid modeling for the multi-criteria decision making of energy systems: an application for geothermal district heating system, Energy 286 (2024) 129590, https://doi.org/10.1016/j.energy.2023.129590. November 2023.
[35] W. Zhong, S. Liu, X. Lin, Y. Zhou, Design optimization and granularity analysis of district heating systems for distributed solar heating access, J. Build. Eng. 57 (July) (2022) 104926, https://doi.org/10.1016/j.jobe.2022.104926.
[36] Z. Yang, et al., Bi-level optimal configuration of renewable electricity based heating in substations of district heating systems, J. Build. Eng. 95 (July) (2024) 110285, https://doi.org/10.1016/j.jobe.2024.110285.
[37] H. Golmohamadi, K.G. Larsen, Economic heat control of mixing loop for residential buildings supplied by low-temperature district heating, J. Build. Eng. 46 (September 2021) (2022) 103286, https://doi.org/10.1016/j.jobe.2021.103286.

[38] M. Abugabbara, S. Javed, H. Bagge, D. Johansson, Bibliographic analysis of the recent advancements in modeling and co-simulating the fifth-generation district heating and cooling systems, Energy Build. 224 (2020) 1–11, https://doi.org/10.1016/j.enbuild.2020.110260.
[39] S. Kuntuarova, T. Lickleder, T. Huynh, D. Zinsmeister, T. Hamacher, V. Perić, Design and simulation of district heating networks: a review of modeling approaches and tools, Energy 305 (June) (2024), https://doi.org/10.1016/j.energy.2024.132189.
[40] P.R. Mazzarino, M. Capone, E. Guelpa, L. Bottaccioli, V. Verda, E. Patti, A modular Co-simulation platform for comparing flexibility solutions in district heating under variable operating conditions, IEEE Trans. Sustain. Comput. (2024) 1–10, https://doi.org/10.1109/TSUSC.2024.3449977, vol. PP, pp.
[41] L. Barbierato, et al., Facilitating smart grids integration through a hybrid multi-model Co-simulation framework, IEEE Access 12 (June) (2024) 104878–104897, https://doi.org/10.1109/ACCESS.2024.3435336.
[42] P. Nageler, et al., Co-simulation workflow for the dynamic modelling and simulation of large-scale district energy systems, Build. Simul. Conf. Proc. 6 (2019) 3698–3705, https://doi.org/10.26868/25222708.2019.211048.
[43] E. Vesaoja, H. Nikula, S. Sierla, T. Karhela, P.G. Flikkema, C.W. Yang, Hybrid modeling and co-simulation of district heating systems with distributed energy resources, 2014 Work. Model. Simul. Cyber-Physical Energy Syst. MSCPES 2014 - Held as Part CPS Week, Proc. (2014) 1–6, https://doi.org/10.1109/MSCPES.2014.6842395.
[44] Economic and environmental viability of central solar heating plants with seasonal storage in the european residential sector: A. Systematic. Multi-objective Optimization. Approach. Victor. Tulus.
[45] H.İ. Tol, TRNSYS from Python 2020 [Online]. Available: https://github.com/DrTol/TRNSYSfromPython, 2020. (Accessed 9 October 2023).
[46] N. Bernier, B. Marcotte, M. Kummert, Calling Python from TRNSYS with CFFI, Dep. Mech. Eng. Polytech. Montréal 6 (2022), https://doi.org/10.5281/zenodo.6523078.
[47] G. Brockman, et al., OpenAI Gym [Online]. Available: http://arxiv.org/abs/1606.01540, Jun. 2016.
[48] V. Tulus, M.H. Abokersh, L.F. Cabeza, M. Vallès, L. Jiménez, D. Boer, Economic and environmental potential for solar assisted central heating plants in the EU residential sector: contribution to the 2030 climate and energy EU agenda, Appl. Energy 236 (November 2018) (2019) 318–339, https://doi.org/10.1016/j.apenergy.2018.11.094.
[49] P. Gluch, H. Baumann, The life cycle costing (LCC) approach: a conceptual discussion of its usefulness for environmental decision-making, Build. Environ. 39 (5) (2004) 571–580, https://doi.org/10.1016/j.buildenv.2003.10.008.
[50] M.H. Abokersh, M. Vallès, L.F. Cabeza, D. Boer, A framework for the optimal integration of solar assisted district heating in different urban sized communities: a robust machine learning approach incorporating global sensitivity analysis, Appl. Energy 267 (April) (2020) 114903, https://doi.org/10.1016/j.apenergy.2020.114903.
[51] H.J. Kluppel, ISO 14041: environmental management - life cycle assessment goal and scope definition - inventory analysis. Editorial, Int. J. Life Cycle Assess. 3 (6) (1998) 301, https://doi.org/10.1007/BF02979337.
[52] Ecoinvent 3.8 dataset documentation 'market for photovoltaic flat-roof installation, 3kWp, multi-Si, on roof-GLO-photovoltaic flat-roof installation, 3kWp, Multi-Si, on Roof.
[53] Y. Elomari, C. Mateu, M. Marín-Genescà, D. Boer, A data-driven framework for designing a renewable energy community based on the integration of machine learning model with life cycle assessment and life cycle cost parameters, Appl. Energy 358 (Mar) (2024), https://doi.org/10.1016/j.apenergy.2024.122619.
[54] H. D. de Santiago E, Arcas-Abella J, Pagès-Ramon A, Larrumbide E, Segmentación del 2019., parque residencial de viviendas en España en clústeres tipológicos. Ministerio de Fomento.
[55] PVGIS data sources & calculation methods - European Commission." Accessed: Jun. 15, 2024. [Online]. Available: https://joint-research-centre.ec.europa.eu/photovoltaic-geographical-information-system-pvgis/getting-started-pvgis/pvgis-data-sources-calculation-methods_en.
[56] Datadis." Accessed: June. 15, 2024. [Online]. Available: https://datadis.es/home.
[57] V. Tulus, D. Boer, L.F. Cabeza, L. Jiménez, G. Guillén-Gosálbez, Enhanced thermal energy supply via central solar heating plants with seasonal storage: a multi-objective optimization approach, Appl. Energy 181 (Nov. 2016) 549–561, https://doi.org/10.1016/j.apenergy.2016.08.037.
[58] Database - Energy - Eurostat." Accessed: November. 1, 2022. [Online]. Available: https://ec.europa.eu/eurostat/web/energy/data/database.
[59] DATADIS. La plataforma de datos de consumo eléctrico, Asociación de Empresas Eléctricas (ASEME) [Online]. Available: https://datadis.es/. (Accessed 4 March 2023).